Hybrid Organic–Inorganic Composites

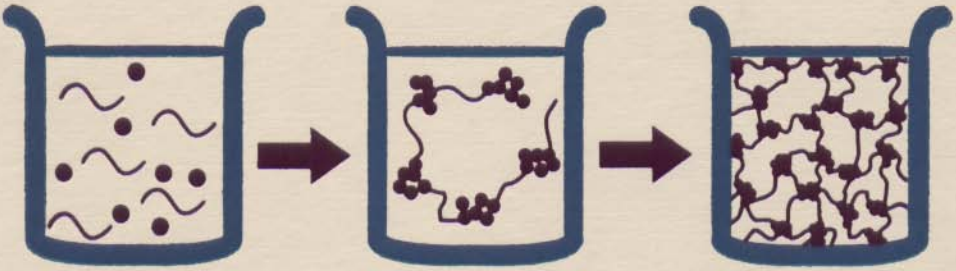

EDITED BY
J. E. Mark, C. Y-C Lee,
and P. A. Bianconi

ACS Symposium Series 585

ACS SYMPOSIUM SERIES 585

Hybrid Organic–Inorganic Composites

J. E. Mark, EDITOR
University of Cincinnati

C. Y-C Lee, EDITOR
U.S. Air Force

P. A. Bianconi, EDITOR
Pennsylvania State University

Developed from a symposium sponsored
by the Division of Polymeric Materials:
Science and Engineering, Inc.,
at the 207th National Meeting
of the American Chemical Society,
San Diego, California,
March 13–17, 1994

American Chemical Society, Washington, DC 1995

Chapter 9

Multiple Size Scale Structures in Silica–Siloxane Composites Studied by Small-Angle Scattering

G. Beaucage[1], T. A. Ulibarri, E. P. Black, and D. W. Schaefer

Sandia National Laboratories, Albuquerque, NM 87185

The physical properties of *in situ* produced composites, such as the TEOS-polydimethylsiloxane hybrids, are related to the complex interaction of structural features from the nano- to macroscopic scales. The nature of these structural interactions is important to understanding and controlling mechanical properties. We believed that the smallest scale structures, in the nanometer range, correlate with properties such as the modulus while large-scale structures in the micron range affect failure in these materials. In this paper we discuss techniques for the analysis of structural features and the interrelation of these features over a wide range of length scales using small-angle light, x-ray and neutron scattering (SALS, SAXS, SANS). The combination of data from a number of different instruments along with a new unified data analysis approach allows for characterization of the interaction between these different structural features.

Hybrid polymer/ceramic materials present a formidable challenge to morphologists. These systems often display multiple structural levels on length scales ranging from Angstroms to millimeters. The combination of small-angle scattering data with fractal approaches has lead to some relief in dealing with these systems. Fractal approaches describe power-law regimes often observed in measured scattering profiles. However, interpretation of such power-law functions is dangerous when self-similar structures exist in narrow size limits (*1*). All real systems are expected to show structural limits to these power-laws. For example, the mass-fractal power-law scattering from a polymer coil displays limits at the overall radius of gyration for the polymer coil and at the persistence length of the polymer chain.

By combining absolute intensity measurements from small-angle light scattering (SALS), ultra-low angle x-ray scattering (*2*) and conventional SAXS (*3*) or SANS (*4*), with diffraction data, morphologies are described from microns to Angstroms. Analysis of such extensive data requires a new approach that accounts for the interaction of structural features at a number of size levels. Although several semi-

[1]Current address: Department of Materials Science and Engineering, University of Cincinnati, Cincinnati, OH 45221–0012

0097–6156/95/0585–0097$12.00/0

empirical equations have been developed to fit length-scale-limited power-law scattering (*5*), none are adequate over five decades in length-scale. Beaucage (*6*), on the other hand, has developed a general equation that is capable of describing scattering functions containing multiple length-scales (Guinier regimes) separated by power-law scaling regimes. This unified approach is applied to scattering data from *in situ*-produced silica/siloxane composites in this paper. The approach is quite general, as can be seen in the examples given from this system, and can be easily applied to other hybrid polymer/ceramic or organic/ceramic systems.

A UNIFIED EQUATION FOR SMALL-ANGLE SCATTERING.

Beaucage (*6*), describes how Guinier's law in exponential-form and structurally limited power-laws can be derived from mutually exclusive scattering events. In the simplest case, the observed scattering is a sum of two components.

$$I(q) \approx G \exp\left(\frac{-q^2 R_g^2}{3}\right) + B\left[\frac{(\mathrm{erf}(q R_g/\sqrt{6}))^3}{q}\right]^P \qquad (1)$$

The first term describes an exponential decay in scattering at a characteristic size, R_g, for one structural level in a material such as phase-separated domains. The second term describes a power-law decay in scattering which follows the exponential regime. The power-law might be due to surface scattering from phase-separated domains whose radius of gyration is described by the first term. Such surface scattering has a limit at low-q described by the error function. $G=N_p \rho^2 V^2$ is the classic Guinier prefactor and B is a prefactor specific to the type of power-law scattering, specified by the regime in which the exponent, P, falls. The momentum transfer, q, has the units $(\text{length})^{-1}$ so large-q scattering probes small length-scales. For Porod's law (scattering from sharp interfaces), for example, P=4 and $B=2\pi\rho^2 S$. For a Gaussian polymer, P=2, and $B = \frac{2\,G}{R_g^2}$ (*6*). For polymeric mass-fractals of arbitrary mass fractal dimension, d_f, Beaucage (*6*) has shown that B is given by $B = \frac{d_f\, G\, \Gamma(d_f/2)}{R_g^{d_f}}$. This is termed a polymeric constraint (*6*) in analogy to the Debye equation for polymer coils. Generally, for surface fractals 4>P>3, while for mass fractals P<3, and for diffuse interfaces P>4 (*1*). The error function (erf) is available in a number of fitting programs (*7*) or can be calculated using an asymptotic expansion (*8*).

Since the crossover error function incorporates the same parameter (the Guinier radius, R_g), as the exponential term, no new parameters are generated by equation 1 compared to local Guinier and power-law fits. Equation 1 is a good approximation for randomly distributed model structures (spheres, disks, rods, and polymer coils) that display a single length-scale. In order to consider multiple-size-scale structures, however, the high-q, small-size limit to power-law scattering must also be considered.

Accounting for Multiple Structural Levels Using the Unified Approach.

All real power-law scattering regimes are limited by structural features in the material at both the small and large size limits. The large size (low-q) limit is described using the error function term in equation 1. We have used an exponential prefactor to describe the high-q, small-size, structural limit for fractal scaling (*6*). The two size limits to power-law scattering ($qR_{gi} \approx 1$ and $qR_{g(i+1)} \approx 1$) can be described through an extension of equation 1,

$$I(q) \approx \sum_{i=1}^{n} G_i \exp\left(\frac{-q^2 R_{gi}^2}{3}\right) + B_i \exp\left(\frac{-q^2 R_{g(i+1)}^2}{3}\right)\left[\frac{(\mathrm{erf}(q R_{gi}/\sqrt{6}))^3}{q}\right]^{Pi} \quad (2)$$

where n is the number of structural levels observed in the scattering pattern. The first term describes a large-scale structure of average size R_{gi} composed of small-scale structures of average size $R_{g(i+1)}$. The second term allows for mass-, surface-fractal or diffuse-interfacial power-law regimes for the large structure. Using equation 2 we can parameterize scattering from a system with multiple-size-scale features. It should be noted that, although equation 2 appears cumbersome, no new parameters have been introduced over local fits using Guinier exponentials and power-laws. Equation 2 can be extended to describe an arbitrary number of interrelated structural features at different size-scales. Such extensions, however, can only be justified when data extends over many decades in q.

Figure 1 is a combination of light scattering (*9*), ultra-low-q SAXS and pinhole SAXS data from a 1% suspension of a conventional fumed silica filler (Hi-Sil 233®) in a rubber matrix. The expanding lines in the structural models of figure 1 indicate magnifications to the next structural-level of the material in decreasing size from left to right. The data has been fit using equation 2 as shown by the dotted line that runs

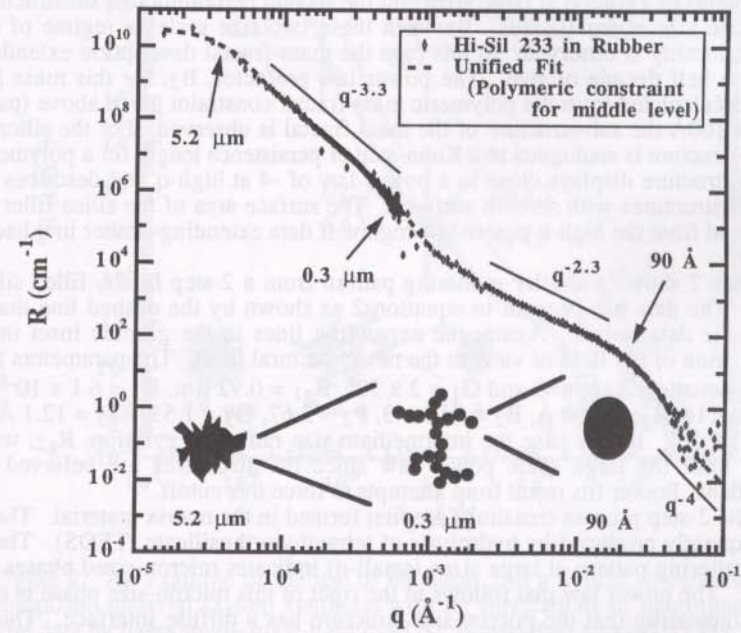

Figure 1. Small-angle light, Bonse-Hart x-ray, and pinhole x-ray scattering for a conventional silica filler (Hi-Sil 233®) in a polymer matrix. The fit is to equation 2 with n=3. The expanding lines in the structural model at the bottom indicate magnifications to the next structural level. These structural levels act as limits to the observed power-laws.

through the data points. The conventional filler displays three levels of structure in the size-range observed. The parameters for the fit using equation 2 are n=3 and G_1 = 3.4 x 10^{10}, R_{g1} = 5.2 μm, B_1 = 2 x 10^{-5}, P_1 = 3.3, G_2 = 9500, R_{g2} = 0.28 μm, B_2 = 0.0023, P_2 = 2.3, G_3 = 69, R_{g3} = 90 Å, B_3 = 8.5 x 10^{-7}, P_3=4.

At large sizes, in the light scattering regime (left), 5 μm aggregates of the filler are observed. In the log-log plot of absolute intensity or Rayleigh ratio (*10*), R, versus q an average structural size is observed as a knee in the scattering pattern. This knee corresponds to a region of exponential decay in scattering where Guinier's Law, or the first term in equations 1 and 2, applies. These 5 μm aggregates can be described as fractally rough particulates over a decade of size. Fractally rough surfaces display power-law scattering with a slope of -3 to -4. At about 0.5 μm this description begins to fail. At this point the radius of gyration of a mass-fractal structure is observed as a second knee in the scattering pattern. Since R_{g2} describes the limit of the low-q power law it is assumed that the large structures are composed of the intermediate-scale mass fractals. The unified approach is the only technique capable of demonstrating this relationship.

Mass fractals display power-law scattering with a slope generally in the range of -1 to -3. The slope of the power law decay is equal to the negative of the mass fractal dimension. An analogy can be made between this branched mass-fractal structure and a branched polymer chain. Both display two size scales, one pertaining to the overall radius of gyration at large sizes and the second pertaining to a substructural or monomeric size at small sizes. Between these two size scales a regime of mass-fractal scattering is observed. In this case the mass-fractal description extends over one and a half decade of size. The power law prefactor, B_2, for this mass fractal regime is calculated from the polymeric mass fractal constraint given above (page 2). At about 100Å the sub-structure of the mass fractal is observed. For the silica filler this sub-structure is analogous to a Kuhn-step or persistence length for a polymer coil. The sub-structure displays close to a power-law of -4 at high-q that describes 100Å glass sub-structures with smooth surfaces. The surface area of the silica filler could be obtained from the high-q power-law regime if data extending further in q had been obtained.

Figure 2 shows a similar scattering pattern from a 2-step *in situ* filled siloxane sample. The data has been fit to equation 2 as shown by the dashed line that runs through the data points. Again, the expanding lines in the graphic inset indicate magnification of the field of view to the next structural level. The parameters for the fit using equation 2 are n=3 and G_1 = 2 x 10^8, R_{g1} = 0.92 μm, B_1 = 6.1 x 10^{-8}, P_1 = 4.2, G_2 = 114, R_{g2} = 150 Å, B_2 = 0.00043, P_2 = 2.67, G_3 = 1.53, R_{g3} = 12.1 Å, B_3 = 0.00027, P_3=4. In this case the intermediate-size radius of gyration, R_{g2}, was not used to limit the large scale power law since the structures are believed to be independent. Poorer fits result from attempts to force this cutoff.

In the 2-step process crosslinks are first formed in the matrix material. The filler is subsequently produced by hydrolysis of tetraethylorthosilicate (TEOS). The knee in the scattering pattern at large sizes (small-q) indicates micron-sized phases in the material. The power law that follows to the right of this micron-size phase is steeper than -4 indicating that the micron-size structure has a diffuse interface. This is in contrast to the fractally-rough interface of the micron-size fumed-silica structure in Figure 1.

Figure 3 describes the difference between a diffuse interface with a power law steeper than -4 and a fractally rough interface with a power law shallower than -4. In the diffuse case, a plot of composition versus angle is constant at a given distance from the center of a spherically symmetric particle. A plot of composition versus radial distance shows a monotonic decay. For a fractally rough particle the angular composition plot shows random discontinuities near the surface while the radial composition plot shows a single sharp transition from the particle phase to the matrix phase.

The power-law scattering regime, that indicates diffuse-surface scaling, extends over a larger range of q than the fractally-rough, surface-scaling-regime in the conventional fumed silica (figures 1 and 2). At about q = 0.01 $Å^{-1}$ a weak second knee is observed in the scattering pattern that describes a structure whose radius of gyration is about 150 Å. As noted above, R_{g2} is not used to cut off the low-q power law from level 1 in the fit. From kinetic studies it is known that the micron scale structure is present long before nanoscale features become apparent. This indicates that the micron and nanoscale features are independent.

The power-law regime corresponding in size to between R_g = 150 and 12 Å reflects a mass fractal structure for the R_g = 150 Å domains. Because the slope is steeper than the mass-fractal power-law slope observed for fumed silica it can be said that the domains are similar in morphology but more ramified or branched than those observed in fumed silica. The polymeric constraint (page 2) was used to limit the power law prefactor in the mass fractal regime of the fit in figure 2. The *in situ*-formed mass-fractal structure has a much smaller overall radius of gyration when

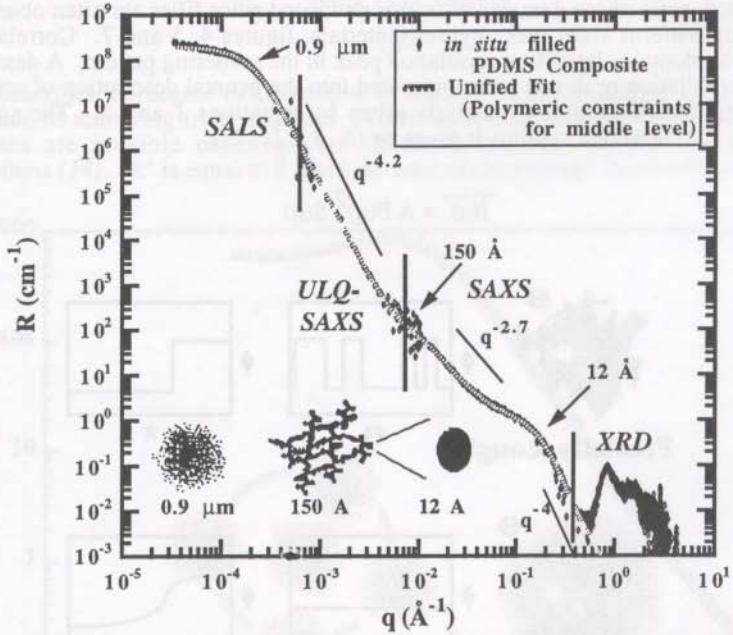

Figure 2. An example of the use of equation 2 in a hybrid silica/siloxane composite material (2-step synthesis with no correlations of nano-phases). The data includes small-angle light (SALS), Bonse-Hart x-ray (ULQSAXS), pinhole x-ray (SAXS) and diffraction data in transmission mode (XRD). The expanding lines in the structural model indicate magnification to the next structural-level in the material. The material displays structural features on three size scales and has fairly well behaved mass scaling behavior that separates these size scale regimes.

compared with Hi-Sil 233. Similarly, the sub-structure of the intermediate mass-fractal aggregate displays a smaller radius of gyration when compared with the conventional filler of figure 1. The mass-fractal scaling regime for the *in situ* filled material of figure 2 is otherwise similar to that of conventional fumed silica. At highest-q the diffraction regime is observed. The humps in this regime correspond to the amorphous halo of PDMS combined with the amorphous halo of the silica filler. The smaller sub-structural elements in the *in situ* filled system are expected to lead to a much higher surface area when compared with the conventional filler.

The high-q limit to the application of equations 1 and 2, that is the limit to the small angle scattering regime, is experimentally reached when the amorphous halo of the diffraction regime begins to dominate the scattering pattern. This is seen in figure 2 at about $q = 0.6$ Å^{-1}. This corresponds to a Bragg size, $2\pi/q$ of about 10 Å. This is the limit to the point-scatterer approximation that is implied in equations 1 and 2.

Correlated Systems

Correlated, nano-phase domains of *in situ* produced silica filler are often observed in scattering patterns from these hybrid-materials, figures 4, 5 and 7. Correlation of these filler domains leads to a correlation peak in the scattering pattern. A description of this correlation peak can be incorporated into the general description of scattering from structurally complex materials given by equations 1 and 2. The scattered intensity for correlated systems is given by (*6, 11, 12, 13*),

$$\overline{I(q)} = A\,F(q)^2\,S(q) \qquad (3)$$

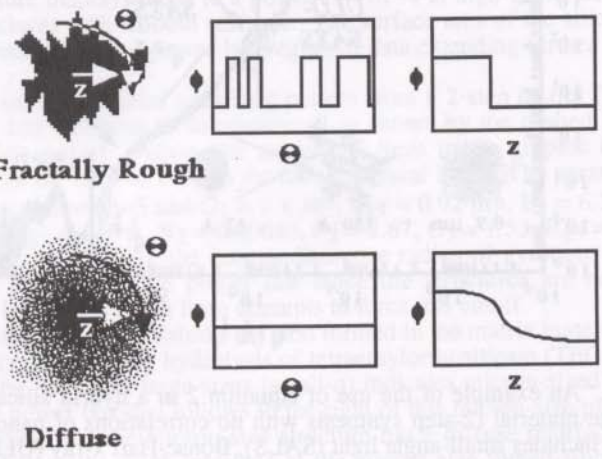

Figure 3. Demonstration of the difference between a diffuse and a fractally rough interface. Schematic plots are of composition, ϕ, versus radial angle, θ, at a fixed radial distance close to the surface and of composition versus radial distance from the center of mass, z.

where "A $F(q)^2$" corresponds to the scattered intensity for non-correlated domains of equation 1 and S(q) is a factor that accounts for weak correlations of the domains. In modifying equation 2 to account for correlations, S(q) is used to modify the two terms of a single structural level. The remaining structural levels are not effected by S(q).

We have previously used a semi-empirical function based on Born-Green theory for S(q) which describes correlations of colloidal particles or domains in terms of a radius of correlation, ζ, and a packing factor, k (*11*, *12*, *13*),

$$S(q) = \frac{1}{1 + k\,\theta} \tag{4}$$

where θ is the "form factor" for structural correlations occurring at an average radial distance ζ (*13*),

$$\theta = 3\,\frac{\sin(q\zeta) - q\zeta\cos(q\zeta)}{(q\zeta)^3} \tag{5}$$

and k describes the degree of correlation ($0 < k < 5.92$). Equation 5 describes the amplitude of scattering from a sphere. Substitution of more complicated amplitude functions are possible under special circumstances such as with very strong correlations (*14*). "k" is equal to 8 times the ratio of the average "hard-core" volume

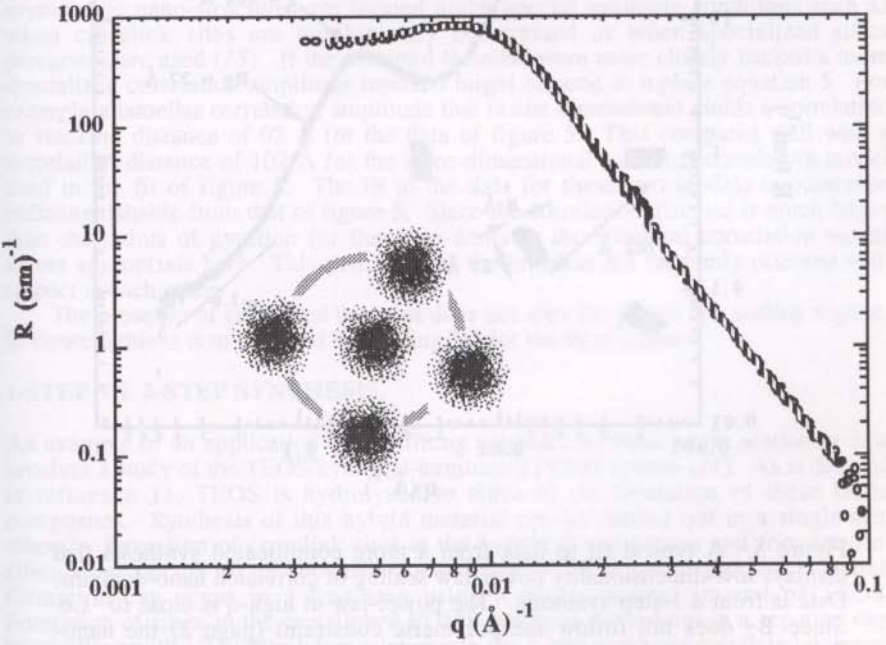

Figure 4. Fit of equation 3 (dashed line) to SANS data (circles) from an *in situ*-filled siloxane rubber with a precursor PDMS molecular weight of 18 kg/mole. Data is from a 1-step synthesis. The structural model (inset) indicates correlated particulates with diffuse interfaces. The shaded circle in the structural model is at a distance ζ from the central particle.

of a domain, v_0, to the average-volume available to the domain. v_1. The maximum value of k, 5.92, is obtained by calculation of this ratio for hexagonal or cubic close-packed crystal structures. In this model the average-volume available to a domain is the volume not occupied by other similar domains divided by the number of domains in the scattering volume. For application of equations 1 and 2 in equation 3, k must have a low value, $k < 4$, consistent with weak correlations. Weakly correlated systems are sufficiently random that the ideas discussed above concerning uncorrelated systems are adequate. Weakly correlated particles are expected to display two size scales, ζ, the average Bragg-like spacing between domains and the radius of gyration, R_g, for the domains. Generally, $R_g \leq \zeta$. ζ corresponds well with the Bragg-spacing of $2\pi/q_{max}$ where q_{max} is the value of q for the maximum peak intensity. This approach is applicable to correlated particulate and spinodal morphologies. It can not distinguish between these physically different morphologies.

Equation 3 can be used to determine the correlation distance and the average size of the filler domains as well as the surface characteristics of the filler (*11*). Figure 4 shows a typical fit (dashed line) to data from an *in situ* filled silica-siloxane

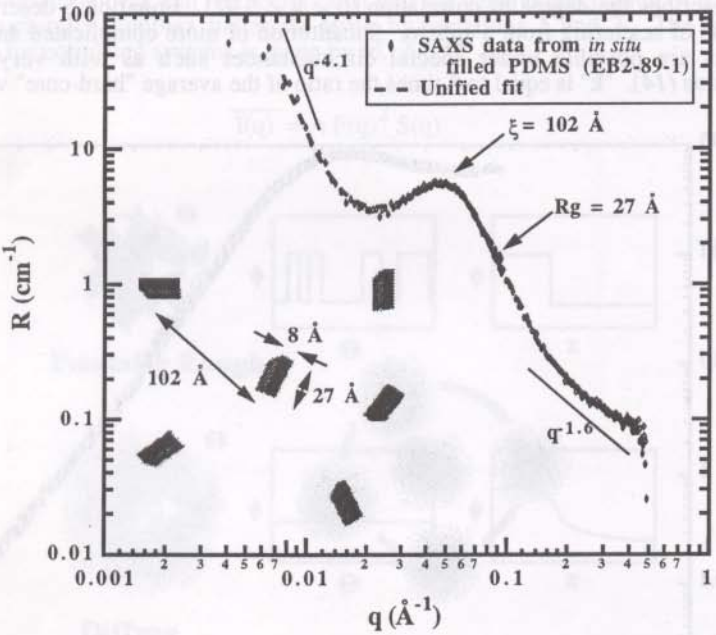

Figure 5. A typical fit to data from a more complicated synthesis that displays low-dimensionality power-law scaling of correlated nano-domains. Data is from a 1-step synthesis. The power-law at high-q is close to -1.6. Since B_2 does not follow the polymeric constraint (page 2) the nano-domains are probably asymmetric. This is shown in the structural model, inset.

composite prepared in a 1-step synthesis. The q-range of this data is much smaller than the data of figures 1 and 2. In the data of figure 4 only the nano-scale features are observed. The schematic representation of this nano-structure, shown in the inset, shows an average correlation distance indicated by the shaded ring of radius ζ and a particulate domain morphology. As mentioned above, equation 3 could also describe a spinodal structure. The correlation distance for the fit is ζ=532±1Å, degree of correlation k=1.99±0.01, R_g=166.1±0.2 Å, G=1508±4 cm^{-1}, P=4.24, B=2.23e-6 cm^{-1}. Since P is greater than 4 the nano-phase/matrix interface is diffuse.

In a 1-step synthesis crosslinking of the matrix and formation of the filler occur simultaneously. The 1-step synthesis characteristically leads to correlation of the nano-scale domains. These correlated domains occur either as diffuse-interfaced structures as evidenced by a power-law steeper than -4 (figure 4) or as low-dimensionality structures with power-laws between -1 and -2.8 as shown in figure 5. The dashed line in figure 5 is a fit to equation 2 using equation 3 to modify structural level 2. Levels 1 and 3 are not modified by equation 3. The parameters for the fit using equations 2 and 3 (for level 2) are n=3 and $B_1 = 5.3 \times 10^{-8}$, $P_1 = 4.1$, $G_2 = 8.1$, $R_{g2} = 26.8$ Å, $B_2 = 5.3 \times 10^{-8}$, $P_2 = 1.57$, $k_2 = 2.2$, $\xi_2 = 102$ Å, $G_3 = 0.12$, $R_{g3} = 8.1$ Å. G_1 and B_3 are 0 since the low-q Guinier and high-q power law are not observed. Since B_2 does not follow the polymeric mass-fractal constraint (page 2) the substructure is probably asymmetric. For example a rod structure would yield a power-law slope of -1 while a lamellar or platelet structure a power-law slope of -2. Beaucage (6) has termed these structural or apparent mass fractals. In this case the structure could be distorted lamellae as shown in the inset of figure 5. These asymmetric nano-structures are formed under special synthetic conditions such as when crosslink sites are topologically constrained or when specialized silica precursors are used (*15*). If the distorted lamellae were more closely packed a more specialized correlation amplitude function might be used to replace equation 5. For example a lamellar correlation amplitude that is one dimensional yields a correlation or stacking distance of 92 Å for the data of figure 5. This compares well with a correlation distance of 102 Å for the three-dimensional spherical correlation model used in the fit of figure 5. The fit to the data for these two models is otherwise indistinguishable from that of figure 5. Since the correlation distance is much larger than the radius of gyration for the nano-domains the spherical correlation model seems appropriate here. This assumes that the lamellae are randomly oriented with respect to each other.

The presence of correlated domains does not alter the power law scaling regime. In figure 6 this is demonstrated by varying "k" for the fit of figure 4.

1-STEP VS. 2-STEP SYNTHESIS.

An example of an application of this fitting approach to small-angle scattering data involves a study of the TEOS/hydroxyl-terminated PDMS system (*11*). As is detailed in reference 11, TEOS is hydrolyzed to silica in the formation of these insitu composites. Synthesis of this hybrid material can be carried out in a single-step whereby formation of crosslink sites at the hydroxyl end-groups and formation of silica filler occurs simultaneously. Alternatively, in a 2-step process crosslink formation can occur in a first step using a stoichiometric amount of TEOS. Formation of silica in the crosslinked PDMS matrix is carried out in a separate step by swelling with a TEOS/catalyst mixture. In the 1-step synthesis correlated domains are generally observed. Data are fit using equation 3. The packing factor, "k", is generally close to 2 indicating weak correlations, figures. 4, 5 and 7. In the 2-step synthesis the domains are generally less correlated. In this case, data can be fit with a non-correlated model, equations 1 or 2, figures 2 and 8.

For the 1-step synthesis the radius of gyration for the nano-domains, determined using equation 3, scales with the molecular weight of the precursor hydroxyl-

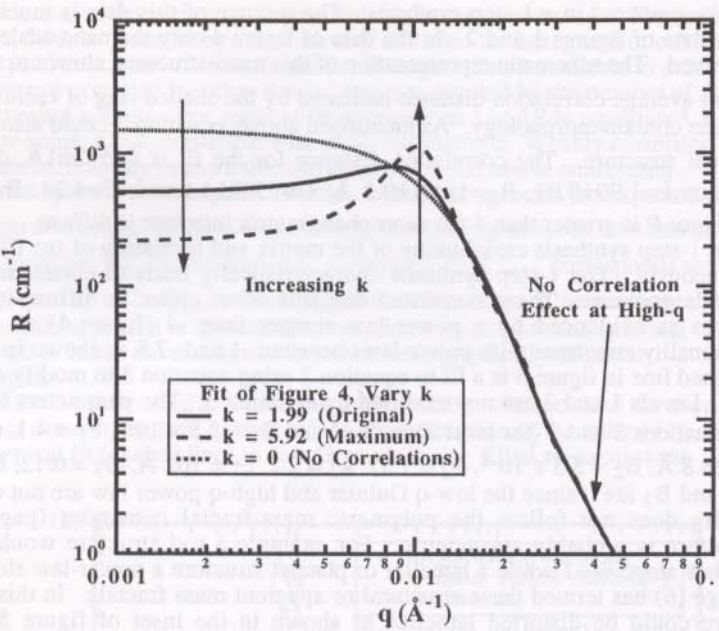

Figure 6. Demonstration of the effect of varying the packing factor "k" on the scattering pattern for the data of figure 4. Packing of the domains does not affect the power-law scaling regime at high-q.

terminated PDMS raised to a power of about 0.3 to 0.4 depending on the amount of catalyst present, figure 9. For the 2-step synthesis, in which crosslinks are first formed followed by swelling with the glass precursor and *in situ* formation of the filler, the radius of gyration follows a much weaker power-law dependence on molecular-weight especially at high loading levels, figure 10.

There are at least two explanations for the observed differences between the 1-step and the 2-step synthesis (*11*). The simplest explanation is that in the 1-step synthesis hydroxyl end-groups on the PDMS chains, serve as nucleation sites for the formation of silica domains. These hydroxyl groups eventually form crosslink sites whether in the precipitated silica phase or in the PDMS phase. Partially hydrolyzed-TEOS and water are expected to be selectively attracted to regions rich in the hydroxyl end-groups where an alcohol-like environment is found. The end-to-end distance for a Gaussian polymer scales with molecular weight raised to a power of 1/2. When filler particle nucleation is limited to chain-end-bound crosslink sites, the amount of silica precursor available for filler growth is proportional to the average volume associated with a crosslink site. The volume of a filler particle would be proportional to the molecular weight to the 3/2 and the radius of the particle proportional to the molecular weight to the 1/2. If a small number of nucleation sites are not associated with chain ends the molecular weight dependence is expected to be weaker. This is especially the case at the low-crosslink density, high-precursor-molecular-weight end of the spectrum. This model is termed the chain-end model.

Depletion of the solution of reacting TEOS enhances the correlation of the filler

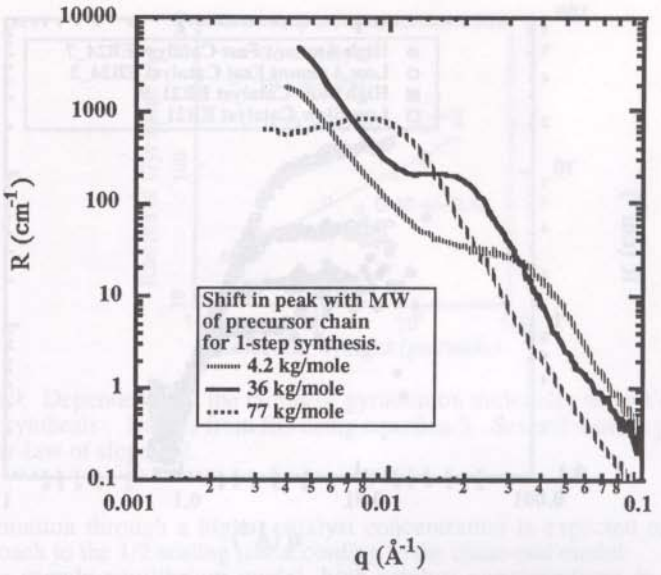

Figure 7. Small-angle neutron scattering data from a 1-step synthesis varying molecular weight of the precursor PDMS. Nano-phases in the 1-step synthesis are typically correlated as indicated by the correlation peak. Correlated data is fit using equation 3 (not shown). The power law at high-q indicates diffuse-interfaced domains.

phase. Where end-groups are close, filler particle growth is limited by the amount of TEOS available. Growth is encouraged where chain-ends are well separated due to ample supply of TEOS. Ionic repulsion may also play a role in the development of correlations.

In the chain-end model, preformed crosslink sites are sterically unfavorable sites for the formation of silica filler particles. This is the case for the 2-step synthesis. In the 2-step synthesis the formation of the filler phase is not intimately related to the network. Because of this only a weak dependence on the precursor molecular weight is expected. Nucleation of silica domains would occur at incidental heterogeneous nucleation sites of which there are fewer especially in the low PDMS molecular-weight-end of the spectrum. Thus one might expect larger particles compared to the 1-step synthesis at high crosslink-densities (figures 9 and 10).

An alternative explanation (*11*) for the relationship between filler size and network molecular weight involves the rubber elasticity of the network. This approach is based on the work of de Gennes concerning phase-separation in a crosslinked polymer/polymer system (*16*). de Gennes and later Bettachy (*17*) introduce a term describing the elasticity of the network into the free energy. This term opposes large-scale phase-separation. The elasticity term leads to the prediction of a correlated phase-separated structure at early stages. The correlation distance is expected to scale with the square-root of the molecular-weight between crosslinks due to the elasticity term. This would lead to a correlation peak in the scattering pattern that is expected to scale with the molecular-weight to the 1/2.

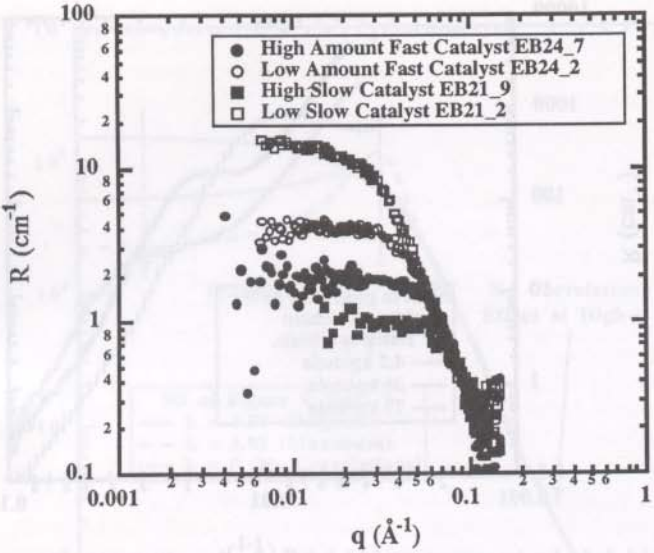

Figure 8. Small-angle neutron scattering from a 2-step synthesis showing the absence of significant phase correlation. Non-correlated data is fit using equations 1 or 2 (not shown). The power law at high-q indicates diffuse-interfaced domains. Data courtesy C. C. Han, B. Bauer to be published.

In the hybrid system the growing glass phase excludes the PDMS network. In this way an analogous condition to that of the de Gennes model exists in which the elasticity of the network might inhibit large-scale phase-separation. Since this explanation for correlations of domains is based on a thermodynamic approach it is termed a pseudo-equilibrium model here. For the pseudo-equilibrium model the association between network elasticity, phase-size and correlation distance would be expected to be most evident in the case of the 2-step synthesis. The approach is somewhat obscure in the case of a 1-step synthesis in which crosslink sites form simultaneously with filler domains. Further, the effect of polymer entanglements on this approach is not clear. At high molecular weights, chain entanglements are expected to act as physical crosslinks such that the elasticity of the network and the phase size should plateau at molecular weights above the entanglement molecular weight. For PDMS the entanglement molecular weight is in the tens of thousands of gm/mole. An entanglement effect is not observed in these systems. An argument can be made that in the 1-step synthesis local crosslinks form rapidly and long before network percolation is reached. These local crosslinks might be sufficient to locally restrict the growth of the silica phase.

In the presence of high catalyst concentrations, where the formation of the silica phase occurs at a more rapid rate, the observed scaling of phase-size with molecular weight is closer to $M^{1/2}$ when compared with lower catalyst concentrations for the 1-step synthesis (figure 9). For the chain-end model there is an inherent competition between crosslink formation and silica formation. If crosslinks form first, silica formation at the cross-link sites is sterically inhibited. Acceleration of the silica-

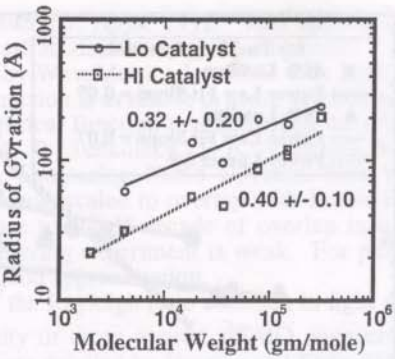

Figure 9. Dependence of the radius of gyration on molecular weight for the 1-step synthesis . Data is from fits using equation 3. Several models predict a power-law of slope 1/2.

domain formation through a higher catalyst concentration is expected to lead to a closer approach to the 1/2 scaling law according to the chain-end model.

For the pseudo-equilibrium model, high catalyst concentrations in the 1-step synthesis leading to faster formation of the silica phase would be expected to lead to less correlated domains and departure from the 1/2 scaling law since the silica formation might out-pace the formation of the network. Data from high and low catalyst concentrations support the chain-end model, figure 9.

The source of correlated phases which scale with molecular weight of the precursor is not resolved. Support for the idea that the glassy phase preferentially forms at chain ends comes from the fact that the 1-step synthesis leads to better correlated phases that more closely follow an $M^{1/2}$ law. Additionally, the observation that higher catalyst concentrations lead to a closer approach to the $M^{1/2}$ law also supports this model. An experiment is suggested whereby the crosslink density is varied through introduction of non-polar crosslinking groups along the chain while retaining hydroxyl terminated endgroups. Through variation in the molecular weight between these non-hydroxyl crosslinking groups the network elasticity could be modified independently of the distance between hydroxyl groups. The end-group model would predict scaling of the particulate size with the molecular weight between hydroxyl groups while the pseudo-equilibrium model would suggest a dependence on the overall crosslink density. We are in the process of carrying out this experiment.

Summary

The unified approach to small-angle scattering (*6*) is useful in examining multiple-size-scale structures in silica/siloxane composites. It was demonstrated that the ideas developed for random structures are also applicable to weakly correlated systems. The unified approach is flexible enough to extract useful information from data in which micro- and nano-structures overlap. This approach is the first to simultaneously account for Guinier scattering and power-law scattering of arbitrary type, i.e. mass-, surface-fractal, Porod or diffuse-interfacial scattering all of which are observed in the in situ-filled siloxane systems.

A discussion of possible sources of correlated phases in *in situ* produced PDMS composites suggests future experiments in which various models for correlated phases can be tested.

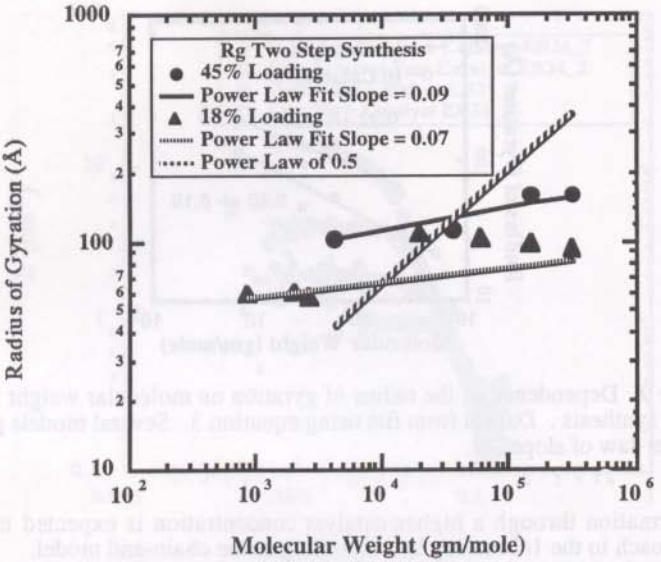

Figure 10. Dependence of the radius of gyration on molecular weight for the 2-step synthesis. In the 2-step synthesis the radius of gyration has a much weaker dependence on precursor molecular weight than in the 1-step synthesis.

Acknowledgments

This work was performed at Sandia National Laboratories supported by the US Department of Energy under contract #DE-AC04-94AL85000.

Literature Cited.

1. See for example the review by Paul Schmidt, Schmidt, P. W. *J. Appl. Cryst.* **1992**, *15*, 567 for a general survey of power-law scattering, seminal work by Porod and Ruland in Porod, G. *Acta Physica Austriaca* **1948**, 2, 133, Porod, G *Kolloid-Z.* **1951**, 124, 83, Porod, G *Kolloid-Z.* **1952**, 125, 51, Porod, G *Kolloid-Z.* **1952**, 125, 108 and Ruland, W. J. Appl. Cryst. **1971**, 4, 70, and references in Korberstein, J. T.; Morra, B.; Stein, R.S., *J. Appl. Cryst.* **1980,** *13* , 34. Also see Debye, P.; Henderson, H. R.; Brumberger, H., *J. Appl. Phys.* **1957**, *28*, 679 and Fischer, M. E.; Burford, R. *J. Phys. Rev.* **1967**, *156*, 583 for references to models of complex systems.
2. National Institute of Standards and Technology beam-line at Brookhaven National Laboratory's National Synchrotron Light Source. G. Long, D. Fischer, G. Beaucage, D. Schaefer.
3. 10-meter small angle x-ray camera at Oak Ridge National Laboratory. J. S. Lin, G. Beaucage, D. W. Schaefer.
4. Sans measurements were performed at Oak Ridge National Laboratory's High Flux Isotope Reactor, National Institute of Standards and Technology's Neutron Scattering Facility and at Los Alamos National Laboratory's LANSCE facility.
5. Lin, J. S. *J. Polym. Sci., Polym. Phys. Ed.* **1990**, *86*, 434.

6. Beaucage G., submitted *J. Appl. Crys.* This approach has been extended to arbitrary polymeric-mass-fractals, Beaucage, G., submitted *J. Appl. Cryst.*
7. For example, "Igor" by WaveMetrics Inc., P.O. Box 2088, Lake Oswego, Oregon 97035. Also the error function is available in some versions of C.
8. For example an empirical function that describes the error function is given in, Press, W. H.; Flannery, B. P.; Teukolsky, S. A.; Vettering, W. T. *Numerical Recipes in C, the Art of Scientific Computing;* Camb. U. Press.: New York, NY, pp. 176.
9. Light scattering data was scaled to overlap with Bonse-Hart x-ray data. This is only possible when close to a half decade of overlap in q is available and when contrast in the light scattering experiment is weak. For purposes of the discussion presented here this is a good approximation.
10. The equivalence of the Rayleigh ratio common in light scattering measurements and the absolute intensity or cross section, $d\Sigma/d\Omega$, measured in neutron and x-ray scattering experiments was detailed by Higgins and Stein, Higgins, J. S.; Stein, R. S. *J. Appl. Cryst.* **1978**, *11*, 346. The Rayleigh ratio is equivalent to the probability that a neutron, for example, will be scattered into solid angle Ω for unit volume of the sample. Absolute intensity in cm^2 can be converted to Rayleigh ratio, which has units of cm^{-1}, by dividing by the irradiated volume. Absolute intensities in cm^{-1} are commonly used at national user facilities since sample and instrumental dimensions are removed by dividing by the irradiated volume. Also see Russell, T. P.; Lin, J. S.; Spooner, S.; Wignall, G. D. *J. Appl. Cryst.* **1988**, *21*, 629.
11. Beaucage, G.; Schaefer, D. W.; Ulibarri, T.; Olivier; B. J., in preparation and short summary of some of this work in MRS Bulletin April 1992 Ulibarri, T.; Beaucage, G.; Schaefer, D. W.
12. Guinier, A; Fournet, G. *Small-Angle Scattering of X-rays*; John Wiley and Sons Inc.: New York, NY, 1955, pp. 42-65. Also see Porod, G. In *Small Angle X-ray Scattering*; Glatter, O.; Kratky, O., Eds.; Academic Press: New York, N. Y., 1982 as well as Feigin, L. A.; Svergun, D. I. *Structural Analysis by SAXS and SANS*; Plenum Press: New York, NY, 1987.
13. Guinier, A.; Fournet, G. *Small-Angle Scattering of X-rays*; John Wiley and Sons Inc.: New York, NY, 1955; pp. 55.
14. We have used a function, θ, based on the form factor for spheres to describe correlations. Since this function is damped by the packing factor, "k", the exact form of this function is not critical when k is small. The spherical function is convenient since it is well behaved and easily interpreted in a physical sense, that is as an average radius of correlation. In highly correlated systems, $k > 4$, the sphere function may become inappropriate, especially when fits to second and higher order peaks are desired. In these cases more specialized functions may be appropriate. We have also used equations 3, 4 and 5 to describe packing effects in filled systems. When k is small, $k < 2$, a peak is not observed but a shift in R_g and G is observed which can be described using this approach, figure 6. It is often necessary to obtain data on a dilute suspension of the filler particle, ≈1%, to used this approach to describe such packing.
15. Ulibarri, T. A.; Black, E.; Loy, D.; Jamieson, G., in preparation.
16. de Gennes, P. G. *J. de Phys. Lett. France* **1979**, *40*, 69.
17. Bettachy, A.; Derouiche, A.; Benhamou, M.; Daoud, M. *J. Phys. I* **1991**, *1*, 153.

RECEIVED September 15, 1994